# Title: Modelling Human Skull Growth: A Validated Computational Model

**Joseph Libby[1], Arsalan Marghoub[2], David Johnson[3], Roman H Khonsari[4], Michael J Fagan[1], Mehran Moazen[2]**

[1]Medical and Biological Engineering, School of Engineering and Computer Science, University of Hull, Hull, HU6 7RX, UK,

[2]UCL Mechanical Engineering, University College London, London WC1E 7JE, UK

[3]Oxford Craniofacial Unit, Oxford Radcliffe Hospitals NHS Trust, John Radcliffe Hospital, Oxford, UK

[4]Hospital Universitaire Necker, Enfants-Malades University Hospital, Paris, France

Corresponding author:
Mehran Moazen, BSc, PhD, CEng
Email: mehran_moazen@yahoo.com; m.moazen@ucl.ac.uk

**Keywords:** human skull growth, finite element, model validation

## Abstract

During the first year of life, the brain rapidly grows and the neurocranium increases to about 65% of its adult size. Our understanding of the relationship between the biomechanical forces, especially from the growing brain, the craniofacial soft tissue structures and the individual bone plates of the skull vault is still limited. This basic knowledge could help in the future planning of cranio-facial surgical operations. The aim of this study was to develop a validated computational model of skull growth, based on the finite element method, to help understand the biomechanics of skull growth. To do this a two-step validation study was carried out. First, an *in vitro* physical 3D printed model and an *in silico* finite element (FE) model were created from the same micro-CT scan of an infant skull and loaded with forces from the growing brain from 0-2 months of age. The results from the *in vitro* model validated the FE model before it was further developed to expand from 0-12 months of age. This second FE model was compared directly to *in vivo* clinical CT-scans of infants without craniofacial conditions (n=56). The various models were compared in terms of predicted skull width, length and circumference, while overall shape was quantified using 3D distance plots. Statistical analysis yielded no significant differences between the male skull models. All size measurements from the FE model vs. *in vitro* physical model were within 5% with one exception showing a 7.6% difference. The FE model and *in vivo* data also correlated well, with the largest percentage difference in size being 8.3%. Overall, the FE model results matched well with both the *in vitro* and *in vivo* data. With further development and model refinement, this modelling method could be used to assist in pre-operative planning of cranio-facial surgery procedures and could help to reduce re-operation rates.

## 1 Introduction

The cranium consists of many bones that are connected together around their periphery by soft tissue structures known as sutures, which are important new bone deposition sites during skull growth and development [1,2]. It is widely accepted that various genetic and epigenetic factors regulate bone formation at the sutures [3-5], with one of the key driving factors for skull growth being provided by the rapidly expanding brain [6-8].

During the early years of life, human brain volume increases rapidly and the cranium undergoes rapid morphological changes in both size and shape, with the neurocranium in particular required to expand to provide protection for the brain [9]. The neurocranium is normally 25% of its adult size by birth, 50% by 6 months and 65% by 1 year, with minimal further growth after 10 years [10,11]. Developmental and growth disorders, as well as some infections, can lead to the occurrence of abnormal skull shapes such as those observed in microcephaly, hydrocephalus and craniosynostosis [12-14].

Understanding the relationship between the biomechanical forces, especially from the growing brain, the soft tissue structures and individual bone plates, and their influence on the growth and shaping of the skulls of infants is clearly important. It would not only help our basic understanding of the biomechanics of normal skull growth, but also be useful in the management of pathological conditions such as craniosynostosis, and in craniofacial reconstruction procedures.

Finite element (FE) method is a powerful numerical technique used to analyse a wide variety of engineering problems [15] and is now becoming increasingly applied in the life sciences to reveal the biomechanical performance of skeletal elements. In brief, this method works by dividing the geometry of the problem under investigation (e.g. a skull) into a finite number of sub-regions, called elements. The elements are connected together at their corners and sometimes along their mid-sides points, called nodes. For stress analysis, a variation in displacement (e.g. linear or quadratic) is then assumed through each element, and equations describing the behaviour of each element are derived in terms of the (initially unknown) nodal displacements. These element equations are then combined to generate a set of system equations that describe the behaviour of the whole problem. After modifying the equations to account for the boundary conditions applied to the problem, these system equations are solved. The output is a list of all the nodal displacements. The element strains can then be calculated from the displacements, and the stresses from the strains.

FE method has the potential to predict the morphological changes during the skull growth. Here, the brain or intracranial volume can be modelled and used to load the overlying cranial bones and joints, to predict overall skull shape. However, FE models need to be validated against laboratory and *in vivo* data to build confidence in their results [16-20]. While there are several studies using FE analysis to model the human infant skull [20-24] to the best of our knowledge no one has attempted to use it to model normal human skull growth.

The overall aim of this study was to understand the biomechanics of skull growth. The specific aim of the study was to develop a validated computational model of skull growth during the early post-natal period (0-12 months) based on the finite element method. This was undertaken in two steps (Figure 1). The first involved a 3D printed physical experimental model (*in vitro*) and matching FE model (*in silico (A)*) both of which were based on a microCT scan of an infant's skull. This set-up was used to test whether the *in silico (A)* could correctly predict the size and shape changes of the *in vitro* physical model under the same loading conditions. In the second step, the FE model was further developed (*in silico (B)*) and compared against a series of patient specific CT (*in vivo*) data (n=56) to predict the

change in cranial size but more importantly overall cranial shape during growth between ages 0-12 months.

## 2 Materials and Methods

### *2-1 Image processing*

An infant skull with an estimated age of 39-42 weeks gestation and unknown sex was scanned in an X-Tek HMX160 microCT scanner (XTek Systems Ltd, Tring, Herts., UK) at the University of Hull at a resolution of 0.132 mm. The resultant stack of two-dimensional images was imported into an image processing software AVIZO (FEI Ltd, Hillsboro, OR, USA) to develop the 3D models. The specimen used to develop the models was loaned from the University of Dundee and was from an archaeological source (skull ID: SC-108). Ethical consent was therefore not required.

The skull was divided into four sections: skull vault bones, cranial sutures, skull base and intracranial volume (ICV). The first section comprised of five cranial bones: two frontal, two parietal and the occipital bone, which were segmented separately. The frontal bones were separated by the metopic (or frontal) suture, which can fuse between 3 and 9 months of age [25]. The sutures and fontanelle were segmented as individual materials to allow for them to be manipulated separately. The skull base consisted of the rest of the occipital bone, both temporal bones, the sphenoid and the 'face' with the respective connecting sutures also segmented individually. The 'face' included the maxillofacial bones (lacrimal, ethmoid, vomer, nasal bones, palatine bones, maxilla and zygomas) and connecting sutures which were all segmented as a single piece due to the study's focus on neurocranial growth. Finally, the ICV was defined as a single material to allow it to be expanded to simulate brain growth. The resultant skull dataset was used to develop both the *in silico* and *in vitro* physical models described in the following sections.

### *2-2 In vitro 3D printed physical model*:

For the first validation phase of the study (*in silico (A)* vs. *in vitro* physical model) the individual bones and sutures of the skull base were combined into a single structure and a solid block was further segmented onto the palate to allow the model to be mounted securely during experimentation.

The segmented skull vault and skull base bone sections were then 3D printed (Stratasys Objet 500, Stratasys Ltd, Edina Prairie, MN, USA). The material chosen to represent the bone was VeroWhitePlus RGD835 (Stratasys Ltd, Edina Prairie, MN, USA) which has a Young's modulus of 3000 MPa, similar to that of infant cranial bone [26]. The cranial sutures were simulated with 1 mm thick elastic thread, a 5 mm length of which was found to have a Young's modulus of 10.38 MPa (measured on a TA Instruments Q800 Dynamic Mechanical Analyser [TA Instruments, DE, New Castle]. This allowed the *in vitro* physical model to expand (Figure 1). Before closure of the skull, a custom made silicone brain-shaped balloon (manufactured from a clay mould of the endocranium) was inserted under the cranial vault. Water was injected into the balloon via a syringe to increase its volume to the ICV values of infants aged 0, 1 and 2 months (using data reported by [27]). These values were 408 ml, 507 ml and 581 ml for females, and 476 ml, 569 ml and 651 ml for males [27]. Before water was added, the system was primed to remove the air. Sensitivity tests regarding the repeatability of the model found a standard deviation of ±1.9% in the measurements recorded. At the end of each volume expansion the *in vitro* physical model was scanned by microCT, so that the geometries could be compared with the *in silico (A)* predictions.

### *2-3 In vivo CT skull data set*:

For the second part, anonymous clinical CT data from 56 infants (see Appendix Tables 1 & 2) were obtained from Necker – Enfants – Malades University Hospital in Paris (Assistance Publique – Hôpitaux de Paris, Université Paris Descartes). This observational study was approved by a local ethical committee (CPP 'Ile-de-France VIII', Hôpital Ambroise Paré, Boulogne-Billancourt, France). The population was aged from < 1 day old to 11 months and 27 days old, with 27 males and 29 females. The most common reasons for the head CT scan were minor trauma (n = 11 males, n = 12 females), followed by epilepsy (n= 4 males, n = 2 female) and nausea (n = 2 males, n = 4 females). In all cases, the brain and skull were judged to be normal. Skulls in this dataset were similarly reconstructed using AVIZO. 'Average' skulls were found (based on length, width and circumference measurements) for each month of age for use as a direct comparison with the *in silico (B)* model. There were however, no male skulls that came within the 10 months and 12 months old age category, and no 8 months old female skulls.

### *2-4 In silico finite element models*:

Two FE models were developed in this study based on the infant skull described in Section 2-1. The first (*in silico (A)*) was used for comparison with the *in vitro* physical model (Section 2-2) and the second (*in silico (B)*) for comparison with the *in vivo* data (Section 2-3). In both cases, the 3D geometries were converted into a tetrahedral mesh using AVIZO, for input into ANSYS finite element software (ANSYS 17 Mechanical, ANSYS, Inc., Canonsburg, PA, USA) as quadratic tetrahedral elements. Mesh convergence was performed by increasing the number of elements and observing the convergence of the results in the normal way. The final models had over 1,040,000 elements. All sections in this model were assigned isotropic material properties.

In the first FE model (*in silico (A)*) a value of 3000 MPa was specified for the Young's modulus of the VeroWhitePlus RGD835 'bone' material, with 100 MPa specified for the ICV, modelled as a brain/dura mater composite, found through sensitivity tests. With the *in vitro* physical model, elastic thread was used to simulate the cranial sutures, which had a Young's modulus of 10.38 MPa (see Section 2-2). The individual threads were originally modelled using LINK (spring) elements however, after conducting sensitivity tests this modelling approach was found to have little effect on the predictions of skull expansion when compared to equivalent SOLID elements. Therefore, the SOLID elements which were already in place from the imported tetrahedral mesh were used to model the sutures. Where multiple thread strands were used in the physical model, the modulus of the equivalent area of suture in the *in silico (A)* model was calculated accordingly. A Poisson's ratio of 0.3 was used for bone [28] and 0.48 for the elastic thread material and ICV. The ICV was prevented from expanding through the foramen magnum and airways by constraining the material in the perpendicular at these points, with the skull being constrained in all directions at the block on the cranial base and loaded via an equivalent thermal expansion of the ICV material (initial volume = 358 ml). To simulate brain growth, increasing thermal expansion was specified for the ICV material in the *in silico* models to increase its volume. An isotropic linear expansion was assumed to generate the expansion of the brain material using the following standard equation:

$$\Delta V = V_1 \times \alpha \times \Delta T \quad (1)$$

where α is the expansion coefficient, ΔV the change in volume, equal to the target volume of the next age $V_2$ minus the current volume $V_1$. The change in temperature ΔT was set at an

arbitrary constant value of 100°C, and α then calculated to give the necessary volume change. The target volumes were determined from literature values [27] for the *in silico (A)* vs. *in vitro* physical model, with actual ICV values determined from the patient CT scans for the *in silico (B)* vs. *in vivo* skulls. In this way, the ICV material was expanded at each age simulating the growth of the brain. To facilitate comparison between the *in vitro* physical and *in silico* (*A*) models, both were aligned using the fixed block on the skull base.

In the second FE model (*in silico (B)*), used for validation with the *in vivo* CT data, the material properties for cranial sutures were updated and the cranial base was modelled as individual bones and sutures (these were all assumed as one piece in, *in silico (A)* - see Figure 1). The same material properties, as *in silico (A),* were used for the bone and ICV, with a Young's modulus of 30 MPa and Poisson's ratio of 0.3 specified for the sutures [29,30]. The ICV was expanded in the same way with similar constraints at the foramen magnum and airways, while the skull was constrained at the basilar part of the occipital bone. The model was loaded via thermal expansion of the ICV at intervals of 0, 1, 2, 3, 4, 5, 6, 7, 8, 9, 11 months of age for males and 0, 1, 2, 3, 4, 5, 6, 8, 9, 10, 11, 12 months for females with the target expansion values taken from the average skulls of the clinical CT data set (Section 2-3). The average skulls for each group had ICVs of 395 ml, 521 ml, 608 ml, 801 ml, 840 ml, 769 ml, 878 ml, 925 ml, 920 ml 912 ml and 1017 ml for male skulls, and 399 ml, 635 ml, 692 ml, 702 ml, 772 ml, 790 ml, 818 ml, 899 ml, 915 ml, 956 ml, 945 ml and 1030 ml for the females corresponding to each age interval. Unlike the previous validation study, there was no common alignment point for the *in silico (B)* models and *in vivo* data. Cephalometric analysis involves using anatomical landmarks that are mostly located on the face of the patient. One of the most frequently used reference planes is the Frankfort horizontal plane, which is taken from the most inferior point on the lower part of the bone orbit to the most superior point of the external auditory meatus [31]. The face of the *in silico (B)* model, however, does not increase in size. Thus, to take the position of the lower orbits would not be an accurate position of where they should be. Therefore, the *in silico (B)* model and the *in vivo* skulls were orientated along the Nasion, the most anterior point of the frontonasal suture, and the Subspinale which is the deepest point on the concave outline of the upper labial alveolar process [31]. Once the skulls had been orientated in the correct planes they were then aligned with one another using the centroids of the basilar part of the occipital bone on the skull base. This bone was chosen as it does not change its relative position in the skull during the first few years of growth [9].

### *2-5 Analysis of size and shape changes*

For every skull model (*in silico (A & B), in vitro* physical model, and the *in vivo* CT scans) the size and shape of the cranial vault was recorded. For size measurements the maximum length, width and circumferences of the skulls were taken and used for comparison with their corresponding skull as mentioned in the previous sections. For the *in silico (B)* vs. *in vivo* study we conducted additional statistical analysis via a non-parametric pairwise test (Wilcoxon signed ranks test) to test for differences between the paired data (e.g. *in vivo* width vs. *in silico (B)* width etc.). A Bonferroni correction was applied to avoid the accumulation of statistical error. All of the statistical analysis was done in R (R Development Core Team, 2012). We did not conduct any statistical test on the *in silico (A)* vs. *in vitro* physical model as the data we had collected was too small for any meaningful statistical result to be found. Therefore, the percentage differences in the widths, lengths and circumferences at each age were calculated. The percentage differences were also calculated for the *in silico (B)* vs. *in vivo* data.

3D distance plots were created using AVIZO to quantify the change in shape and to visualise the differences between the skulls. Models were aligned with one another and the points on the first surface mesh were measured to the closest point on the second surface. The areas at which the two surfaces differed (both positively and negatively) could be clearly seen and used to show where the *in silico* models over or under-predicted skull growth. The maximum differences (mm) in both the positive and negative directions were calculated and used on the colour map scale.

## 3 Results

The results of our analysis are given for each set of comparisons (Figures 3-6).

### *3.1 In silico (A)* vs. *in vitro physical model (first validation study)*

#### *Size analysis*

When comparing the predicted widths of the skulls (Figure 3), the largest percentage difference between the *in silico (A)* model and *in vitro* models was 3.7% and 4.9% for male and female models respectively. Overall, the male *in vitro* physical model increased in width by 6% compared to 8.9% for the male *in silico (A)* model. The female *in vitro* physical model increased in width by 7.7% while the female *in silico (A)* model increased by 10%. Finally the smallest percentage difference with regards to the prediction in width was observed at the ages of 2 months for females, being 2.5%, and 1 month old for males at 0.6%.

The largest overall difference between the *in silico (A)* and *in vitro* physical models was found when observing the length. The 0 month old male *in silico* model had a difference of only 1.3% compared to 7.6% of the 2 months old male. The largest female difference was less than half of that of the male model being 3.3%, while the smallest difference was 2%. The *in vitro* physical model recorded a change in length of 15.2% and 10.9%, with the *in silico (A)* model increasing by 9.5% and 9.6% for males and females.

All of the *in silico (A)* circumference measurements were within 5% of the measurements recorded by the *in vitro* physical model. The largest difference between for the male models was 4.8% while the smallest was 4.3%. The female model comparisons had a largest difference of 4.9% and smallest being 4.6%. Despite the female *in silico (A)* model producing slightly higher percentage differences, it produced the closest comparable percentage increase for the circumference. The *in vitro* physical model increased by 9.4% for 0-2 months age, while the female *in silico (A)* model, increased by 9.6%.

#### *Shape analysis*

Only the 3D distance plots (Figure 4) of the female skulls are presented due to the male skulls producing similar results. Here the blue areas highlight where the *in silico (A)* model under-predicts the *in vitro* physical model shape after expansion. The red areas show where the *in silico (A)* over-predicted the shape and the green areas display where there is little to no difference between the two models. It is important to note that the colour scale is set individually for each age. While it may appear that the 0 months old *in silico (A)* skull under-predicted the *in vitro* physical skull more than the two months old *in silico (A)* skull due to the larger blue patch on the parietal and occipital bones, this is not the case as shown by the max and min values for the colour scale.

The blue areas located on the posterior part of the parietal bone and the occipital bone, for all ages, correlate to the size measurements taken showing that the *in silico* (*A*) skull does

not grow as much as the *in vitro* physical model at the back of the skull. The *in silico (A)* model over-predicted the *in vitro* physical model towards the front of the skull with the maximum over prediction located above the orbits. Interestingly the *in silico (A)* skull also over predicted the expansion of the width of the skull in the medial-lateral direction. This is most clearly seen when viewing the temporal region on the 1 month and 2 months old skulls.

### *3.2 In silico (B)* vs. *in vivo (second validation study)*

#### *Size analysis*

A comparison of the results of the *in silico (B) model* growth predictions at each of the seven average ages (0, 1, 2, 4, 6, 9 and 12 months) is presented in Figure 5. Values of skull width, length and circumference are shown, for males and females, and compared to the CT data. The large green rhomboid shapes indicate the most 'average' skulls against which the *in silico (B)* models were compared. For the width measurement the largest percentage difference between the average *in vivo* CT skull data and *in silico (B)* models was 6.7% for males and 5.1% for females, at the oldest ages. The smallest differences were only 1.6% for male models located at 0 months age and 0.2% for female models at 9 months of age. When comparing the length of the skulls, the largest difference was observed at 9 months age for the *in silico (B)* male model being 5.4%, and the female models had a maximum difference in length of 4.8% recorded at 1 month age. The smallest difference in the prediction of the length of the skull was 0.2% for the male *in silico (B)* model, located at 6 months age and for the female *in silico (B)* models a difference of 0.4% was recorded at 6 months age. Finally the circumference was compared. Out of the male *in silico (B)* models the largest difference in circumference when compared to the *in vivo* models was 4.2% when comparing the models at the oldest age of 11 months. The predicted greatest circumference difference for the female models was 2.5% found when comparing the *in silico (B)* and *in vivo* skull at 6 months age. The smallest difference in circumference between the *in silico (B)* models and *in vivo* scans were both 0.5% at 4 months age (male models) and 0 months age female models.

#### *Statistical comparison*

The results (Table 1) from the Wilcoxon signed ranks test gave p-values of 0.21, 0.37, 0.10 and 0.21 when testing the male widths, lengths, circumferences and ICV values respectively across all 11 ages. For the females the p-values were 0.22, 0.21, 0.008 and 0.13 for the width, length, circumference and ICV comparisons respectively across the 12 monthly ages. Thus, out of the 8 tests conducted only the female circumference comparison showed a significantly different ($p<0.05$) result between the *in silico (B)* vs. *in vivo* results.

#### *Shape analysis*

The differences in shape between the *in silico (B)* and *in vivo* data sets are shown by 3D distance plots (Figure 6). The differences produced by the male models were not dissimilar to those produced by the female results so only the female skulls are shown. The red areas show where the *in silico (B)* skull over-predicted the *in vivo* skull shape whereas the blue areas show where it under-predicted the *in vivo* skull shape. The area at which the *in silico (B)* is most likely to under-predict the *in vivo* skull is the face. This is not surprising as the face of *in silico (B)* model did not grow. Disregarding the face, the areas of under-prediction differ with age. At 0 months age the height of the frontal bones near the anterior fontanelle are taller in the *in vivo* skull. As the age increases, the area of under prediction tends to move down the frontal bones to just above the orbits indicating that the front of the *in silico (B)* model does not flatten as much as the *in vivo* skulls do. Towards the posterior part of the

skull the areas of under prediction again change with age. From 0-4 months the bony eminences of the parietal bone protrude more than the *in silico (B)* skulls. As the age of the skulls increases the eminences become flatter which reduced the blue areas around this part. It is interesting to note that like the *in silico (A)* model previously, the width of the base of the skull, especially at the temporal bones, is tending towards over prediction. After two months, however, the *in vivo* skull base starts to outgrow the *in silico (B)* model at these areas. While the maximum under-prediction distances appears larger than the maximum over-prediction it should be noted that the colour scales are set individually to each age.

The areas of over-prediction also vary with age. On the 0 month old skull the maximum area of over-prediction is on the left parietal followed by the occipital bone. For the 1 month model these areas move more towards the posterior and anterior fontanelles. At 2 months the anterior fontanelle is the location of the largest over prediction between the models. For the 4 months – 12 months old models the areas stay mostly in the same positions with the main difference being located at the posterior fontanelle while the second highest area remains at the anterior fontanelle.

## 4 Discussion

A series of finite element models were developed to model the rapid skull growth that occurs during the first year of life due in part to the biomechanical forces created by the expanding brain. An FE model (*in silico (A)*) was validated against an *in vitro* physical model which simulated early skull growth. The model was then developed further (*in silico (B)*) to predict growth from 0 to 12 months, and compared to *in vivo* clinical CT data. Both models were validated by comparing both size and shape, with the change in shape being the main focus of the study.

The congruence between the *in silico (A)* and *in vitro* physical models gives confidence in the FE modelling approach, with the measurements predicted at each age being less than 5% of the *in vitro* physical model measurements with one exception of 7.6%. The lowest difference was only 0.6% smaller than the result given by the *in vitro* physical model. Both models had similar shapes when considering the 3D distance plots. The differences between the two models may have been caused by the weight of the water used to expand the skull coupled with a lack of support at the posterior section of the skull in the *in vitro* physical model.

The *in vivo* CT data set was also compared with literature regarding normal skull growth. However, very few studies have been conducted in this area. Dekaban [11] was one such study although, there were some inconsistencies in the results, such as the 1 month old female skull which was smaller than expected. The reasons for this reduction in size were unclear but both the clinical *in vivo* data and the results from another study [32] suggest that the skull continually increases in size during the first year. Disregarding this anomaly, the highest percentage difference was 8.9% observed in the male micro-CT scan at 6 months old. The largest difference in the female micro-CT scan was 7.9%, however, the disparity between the *in vivo* and literature data are most likely to be caused by the unequal values given for the ICV. Also, the results from Dekaban [11] were physical clinical measurements which would have increased the results slightly with the inclusion of hair, skin, muscle tissue etc. This would therefore explain some of the discrepancies with our data.

The comparison between the *in silico (B)* and *in vivo* models, investigated in the second phase of the study, was used to validate the prediction of skull growth up to 12 months of

age. The smallest differences were 0.3% for male and 0.8% female *in silico (B)* model comparison. The largest percentage difference was 8.3% for the male *in silico (B)* model and 5.1% for the female. This is likely to be due to the isometric modelling of brain growth in this study, using the thermal expansion method, where in reality it is an anisotropic phenomena caused by different regions of the brain developing at different rates along with restriction of the growth caused by the fusing sutures [33,34]. This growth of the brain can be seen in the 3D distance plots (Figure 6). As the skull age increases the lambdoid sutures at the posterior part of the skull begin to close in response to the forces rising from the growing brain on the dura mater and the sutures [35]. This gradual bone formation at the sutures restricts the growth in this direction causing the brain to grow perpendicular to the fusing suture.

The positive median differences (Table 1) indicate that on average all of the *in silico (B)* skulls were smaller than the *in vivo* CT scans although this difference is not significant with the exception of the female circumferences. Despite a finding of a significant difference ($p = 0.008$) when comparing the female *in vivo* circumferences against those predicted by the female *in silico (B)* models the largest percentage difference between the measurements taken was 3% (12.9 mm). Therefore, the difference (albeit statistically significant) between the female *in vivo* and *in silico (B)* models is very small. The shape analysis carried out on the skulls also produced small differences. The largest difference recorded was an under-prediction of 18.4mm. This however was located on the face of the skull so it is most likely smaller than this because the study's focus on cranial vault expansion.

In the current model the growth of the skull was achieved by expanding the ICV material to the volume of the next age in monthly stages so that there could be a direct comparison between the models and *in vivo* data. Clinically growth happens as a continual process for normal skulls [10,11,32]. Using a rate of expansion, instead of specific target volumes, could be more appropriate for future models as it would allow for the prediction of the skull growth without knowing the final ICV. Another consideration for future models is brain and ICV volumes in patients with craniosynostosis and the rate at which the brain grows. From the literature, the volume of the brain and ICV of a patient with craniosynostosis depend on the severity and type of fusion. For example, non-syndromic isolated sagittal suture fusion causes larger than average ICV's [36]. Whereas, unilateral coronal synostosis shows no significant difference compared to normal ICV's and brain volumes [37]. Therefore, when trying to model the growth of a synostotic skull such considerations must be taken into account.

One additional approach to quantifying the change in shape would be to use Geometric morphometrics (GM). GM is primarily used in the biological sciences and is the quantitative analysis of biological forms [38]. The process involves placing landmarks (2D or 3D) at specific anatomical points located on the biological form. The problem with using this method to measure the changes in infant cranial vault shape is the lack of anatomical points available. Many of the landmarks found on the human skull are located on the face and cranial base. There are a few exceptions to this; the Bregma and Lambda locations [39-41], however, these are located at the points where the coronal and sagittal sutures intersect (Bregma) and the midline point where the sagittal and lambdoid suture (Lambda) intersect [41] and therefore, will not be in the same position on each infant skull. Li et al. [42] did landmark the infant calvaria without using the landmarks on the cranial face or base, but the method described is very subjective as to the placement of the landmarks along the suture and difficult to replicate. One reason for this is suture fusion rates are different for each person and have different interdigitated patterns from person to person. The method used by Li et al. [42] offers a clever and simple solution to the suture fusion problem by taking

landmarks on either side of the suture and calculating the midpoint. As the sutures fused on the older skulls there would remain a landmark in the centre of the suture. The question still arises however, as to where precisely to place the landmarks along the suture? A more appropriate method to use was presented by Loyd [43], as it removes the errors associated by a user's involvement due to it being an automated process. However, the scope of this work requires an additional research paper.

Even with the close comparisons between these results there were several limitations to our modelling approach,

(1) Alignment of the skulls. As mentioned previously in Section 2.6, cephalometric analysis involves using anatomical landmarks that are mostly located on the face of the patient with the Frankfort horizontal reference plane commonly used [31]. The face of the *in silico (B)* model does not increase in size however. Thus, to use the position of the lower orbits would lead to the two data sets being orientated in different directions and therefore very few meaningful comparisons could be made. For completion and due to it being a well-regarded anatomical plane, 3D distance plots for with the *in silico (B)* models and the *in vivo* skulls aligned in the Frankfort plane can be seen in Appendix 2.

(2) Isotropic expansion of the ICV material. While different sections of the brain are known to grow at different rates [33,34], it would be extremely difficult to incorporate this differential expansion into the model due to the quality of our original CT being unable to detect the soft tissue of the brain so an accurate representation of the morphology of the *ex vivo* skull's brain is not possible.

(3) The model itself consisted of only bone, suture and an ICV material, while no soft tissues (e.g. skin, muscles, or dura mater) were considered.

(4) Only the ICV grew. The cranial bones did not increase in thickness and their shape remained roughly the same during the 12 month expansion. There was also no gradual fusion of the suture material.

The results of this study suggest that further development and application of suitably constructed patient-specific models might be useful with pre-surgical planning for craniofacial surgery procedures, such as in craniosynostosis surgery. Despite the simplifications and limitations of the model, the results are reasonable, and show a good prediction of actual cranial vault growth in both size and shape. Model development and incorporation of more tissue structures can be expected to increase the model's accuracy further. With the approach used here, prediction of the severity of the deformity could be used to aid surgeons with their treatment plans. One consideration when planning for craniofacial surgery is to obtain an age-matched normal skull adapted to the skull dimension of the patient to offer a visual guide as to how best to correct the cranial bones to produce a normal shaped skull [44]. This approach would be of great help in clinical practice by solving the issue of the expected result when preparing skull vault surgery for craniosynostosis and with future development could be used to predict the growth of the skull post-surgery.

## Authors' contribution

JL, MM, MF, DJ and RH designed the study, JL performed the study, JL and AM performed the analysis, JL, MM, MF, DJ and RH wrote the paper. All authors gave final approval for publication.

## Competing interests

The authors have no competing interests.

**Funding.** This work was supported by the Royal Academy of Engineering (grant no. 10216/119 to MM) and the University of Hull (to JL).

## Acknowledgements

We also thank Dr Ali Alazmani Nodeh for his support during the *in vitro* model development, Dr Alex Blanke and Dr Hugo Dutel for their support with the statistical analysis, and the University of Dundee for the loan of the infant skull.

## Data Accessibility

The datasets supporting this article have been uploaded as part of the supplementary material (Appendix 1).

## References

1. Opperman LA. 2000 Cranial sutures as intramembranous bone growth sites. *Dev. Dynam*. **219**, 472-485 (doi: 10.1002/1097-0177(2000)9999:9999<::AID-DVDY1073>3.0.CO;2-F)
2. Herring SW. 2008 Mechanical influences on suture development and patency. *Front. Oral. Biol.* **12**, 41–56. (doi: 10.1159/000115031)
3. Morriss-Kay GM, Wilkie AOM. 2005 Growth of the normal skull vault and its alteration in craniosynostosis: insights from human genetics and experimental studies. *J. Anat*. **207**, 637-653 (doi: 10.1111/j.1469-7580.2005.00475.x)
4. Kimonis V, Gold J-A, Hoffman TL, Panchal J, Boyadjiev SA. 2007 Genetics of craniosynostosis. *Semin. Pediatr. Neurol*. **14**, 150-161. (doi:10.1016/j.spen.2007.08.008)
5. Richtsmeier JT, Flaherty K. 2013 Hand in glove: brain and skull in development and dysmorphogenesis. *Acta. Neuropathol.* **125**, 469-489. (doi: 10.1007/s00401-013-1104-y)
6. Lieberman DE. 2011 Evolution of the human head. London: Harvard University Press.
7. Moazen M, Alazmani A, Rafferty K, Liu ZJ, Gustafson J, Cunningham ML, Fagan MJ, Herring SW. 2016. Intracranial pressure changes during mouse development. *J. Biomech.* **49**, 123-126. (doi: 10.1016/j.jbiomech.2015.11.012)
8. Jin S-W, Sim K-B, Kim S-D. 2016 Development and growth of the normal cranial vault: an embryologic review. *J. Korean. Neurosurg. Soc*. **59**, 192-6 (doi: 10.3340/jkns.2016.59.3.192)
9. Scheuer L, Black S. 2004 The juvenile skeleton. London: Elsevier Academic Press.
10. Sperber GH. 1989 Craniofacial embryology, 4th edition, p. 102. London: Wright, Butterworths.

11. Dekaban AS. 1977 Tables of cranial and orbital measurements, cranial volume, and derived indexes in males and females from 7 days to 20 years of age. *Ann. Neurol.* **2**, 485-491.

12. Ramos da Silva S, Gao S-J. 2016 Zika virus: An update on epidemiology, pathology, molecular biology, and animal model. *J. Med. Virol.* **88**, 1291-96 (doi: 10.1002/jmv.24563)

13. Blaser, SI, Padfield N, Chitayat D, Forrest CR. 2015 Skull base development and craniosynostosis. *Pediatr Radiol.* **45**, S485-96 (doi: 10.1007/s00247-015-3320-1)

14. Johnson D, Wilkie AOM. 2011 Craniosynostosis. *Eur. J. Hum. Genet*. **19**, 369-376. (doi:10.1038/ejhg.2010.235)

15. Fagan MJ. 1992 Finite element analysis: theory and practice. Longmans.

16. Kupczik K, Dobson CA, Fagan MJ, Crompton RH, Oxnard CE, O'Higgins P. 2007 Assessing mechanical function of the zygomatic region in macaques: validation and sensitivity testing of finite element models. *J. Anat.* **210**, 41–53. (doi: 10.1111/j.1469-7580.2006.00662.x)

17. Szwedowski TD, Fialkov J, Whyne CM. 2011 Sensitivity analysis of a validated subject-specific finite element model of the human craniofacial skeleton. *Proc Inst Mech Eng H.* **225**. 58-67. (doi: 10.1243/09544119JEIM786)

18. Gröning F, Bright JA, Fagan MJ, O'Higgins P. 2012 Improving the validation of finite element models with quantitative full-field strain comparisons. *J. Biomech.* **45**, 1498-1506. (doi: 10.1016/j.jbiomech.2012.02.009)

19. Toro-Ibacache V, Fitton LC, Fagan MJ, O'Higgins P. 2016 Validity and sensitivity of a human cranial finite element model: implications for comparative studies of biting performance. *J Anat.* **228**, 70-84. (doi: 10.1111/joa.12384)

20. Lapeer RJ, Prager RW. 2001 Fetal head moulding: finite element analysis of a fetal skull subjected to uterine pressures during the first stage of labour*. J. Biomech*. **34**, 1125-1133. (doi: 10.1016/S0021-9290(01)00070-7)

21. Khonsari RH, et al. 2013 A mathematical model for mechanotransduction at the early steps of suture formation. *Proc R Soc B* 280: 20122670. (doi.org/10.1098/rspb.2012.2670)

22. Roth S, Raul J-S, Willinger R. 2010 Finite element modelling of paediatric head impact: Global validation against experimental data. *Comput Methods Programs Biomed,* **99**, 25-33. (doi: 10.1016/j.cmpb.2009.10.004)

23. Wolanski W, Larysz D, Gzik M, Kawlewska E. 2013 Modeling and biomechanical analysis of craniosynostosis correction with the use of finite element method. *Int J Numerl Method Biomed Eng.* **29**, 916-925. (doi: 10.1002/cnm.2506)

24. Li Z, Luo X, Zhang J. 2013 Development/ global validation of a 6-month-old pediatric head finite element model and application in investigation of drop-induced infant head injury. *Comput Methods Programs Biomed*. **112**, 309-319. (doi:10.1016/j.cmpd.2013.05.008)

25. Vu HL, Panchal J, Parker EE, Levine NS, Francel P. 2001 The timing of physiologic closure of the metopic suture: a review of 159 patients using reconstructed 3D CT scans of the craniofacial region. *J Craniofac Surg*. **12**, 527-32

26. McPherson GK, Kriewall TJ. 1980 The elastic modulus of fetal cranial bone: A first step towards an understanding of the biomechanics of fetal head molding. *J. Biomech*. **13**, 9-16. (doi: 10.1016/0021-9290(80)90003-2)

27. Abbott A, Netherway DJ, Niemann DB, Clark B, Yamamoto M, Cole J, Hanieh A, Moore MH, David DJ. 2000 CT-Determined Intracranial Volume for a Normal Population. *J. Craniofac. Surg*. **11**, 211-223.

28. Gröning F, Fagan MJ, O'Higgins P. 2013 Comparing the distribution of strains with the distribution of bone tissue in a human mandible: A finite element study. *Anat. Rec.* **296**, (doi: 10.1002/ar.22597)

29. Henderson JH, Chang LY, Song HM, Longaker MT, Carter DR. 2005 Age-dependent properties and quasi-static strain in the rat sagittal suture. *J. Biomech*. **38**, 2294-2301. (doi: 10.1016/j.jbiomech.2004.07.037)

30. Moazen M, Peskett E, Babbs C, Pauws E, Fagan MJ. 2015 Mechanical properties of calvarial bones in a mouse model for craniosynostosis. *PloS One*. **10**, e0125757. (doi: 10.1371/journal.pone.0125757)

31. Sato K, Shirakawa T, Sakata H, Asanuma S. 2014 Effectiveness of the analysis of craniofacial morphology and pharyngeal airway morphology in the treatment of children with obstructive sleep apnoea syndrome. *Dentomaxillofacial Radiology*. **41**, 411-416. (doi: 10.1259/dmfr/28710443)

32. Schneider LW, Lehman RJ, Pflug MA, Owings CL. 1986 Size and shape of the head and neck from birth to four years. University of Michigan Transport Research Institute.

33. Paus T. 2005 Mapping brain maturation and cognitive development during adolescence. *TiCS*. **9**, 60-68. (doi: 10.1016/j.tics.2004.12.008)

34. Dubois J, Dehaene-Lambertz G, Kulikova S, Poupon C, Hüppi PS, Hertz-Pannier L 2014 The early development of brain white matter: A review of imaging studies in foetuses, newborns and infants. *Neuroscience*. **276,** 48-71. (doi: 10.1016/j.neuroscience.2013.12.04

35. Tubbs RS, Bosmia AN, Cohen-Gadol AA. 2012 The human calvaria: a review of embryology, anatomy, pathology, and molecular development. *Childs Nerv Syst*. **28**, 23-31. (doi: 10.1007/s00381-011-1637-0)

36. Anderson PJ, Netherway DJ, McGlaughlin K, David DJ. 2007 Intracranial volume measurements of sagittal craniosynostosis. *J. Clin. Neurosci*. **14**, 455-458. (doi:10.1016/j.jocn.2006.07.001)

37. Hill CA, Vaddi S, Moffitt A, Kane AA, Marsh JL, Panchal J, Richtsmeier JT, Aldridge K. 2011 Intracranial volume and whole brain volume in infants with unicoronal craniosynostosis. *Cleft Palate Craniofac J*. **48**. 394-398. (doi: 10.1597/10-051)

38. Utkualp N, Ercan I. 2015 Anthropometric measurements usage in medical sciences, *BioMed Research International*. 404261. (doi: 10.1155/2015/404261)

39. Bruner E, Saracino B, Ricci F, Tafuri M, Passarello P, Manzi G. 2004 Midsagittal cranial shape variation in the genus *Homo* by geometric morphometrics. *Coll Antropol*. **28**, 99-112.

40. Lieberman DE, McBratney M, Krovitz G. 2002 The evolution and development of cranial form in *Homo sapiens*. *PNAS.* **99**, 1134-1139. (doi: 10.1073/pnas.022440799)

41. Martínez-Abadías N, Esparza M, Sjøvold T, González-José R, Santos M, Hernández M. 2009 Heritability of human cranial dimensions:comparing the evolvability of different cranial regions. *J. Anat.* **214**, 19-35. (doi: 10.1111/j.1469-7580.2008.01015.x)

42. Li Z, Park B-K, Liu W, Zhang J, Reed MP, Rupp JD, Hoff CN, Hu J. 2015 A statistical skull geometry model for children 0-3 years old. *PloS One*. **10**, 1-13. (doi: 10.1371/journal.pone.0127322)

43. Loyd AM. 2011 Studies of the Human Head From Neonate to Adult: An inertial, geometrical and structural analysis with comparisons to the ATD head. PhD Dissertation. Department of Biomedical Engineering, Duke University.

44. Chim H, Wetjen N, Mardini S. 2014 Virtual surgical planning in craniofacial surgery. *Semin Plast Surg*. **28**, 150-158. (doi: 10.1055/s-0034-1384811)

**Table 1:** Statistical analysis *in silico (B)* vs. *in vivo*. The results from the Wilcoxon signed ranks test with Bonferroni corrections are given.

| Comparison | Median (mm) | CI (95%) | p-value* |
|---|---|---|---|
| **Male** | | | |
| Width | 4.3 | -1.4 to 8.8 | 0.21 |
| Length | 1.4 | -2.3 to 8.0 | 0.37 |
| Circumference | 8.6 | -2.0 to 14.6 | 0.10 |
| ICV | 0.6 | -0.1 to 0.7 | 0.21 |
| **Female** | | | |
| Width | 0.5 | -2.0 to 0.5 | 0.22 |
| Length | 2.9 | -0.6 to 5.2 | 0.21 |
| Circumference | 7.4 | 4.4 to 9.4 | 0.008 |
| ICV | 0.3 | 0.1 to 0.5 | 0.13 |

* after Bonferroni correction

**Figure 1**: Workflow of the study: Two *in silico* FE models were created with the same microCT scan. The left branch shows the validation with a 3D printed *in vitro* model and the right branch shows some of the *in vivo* CT skulls used to validate a second FE model.

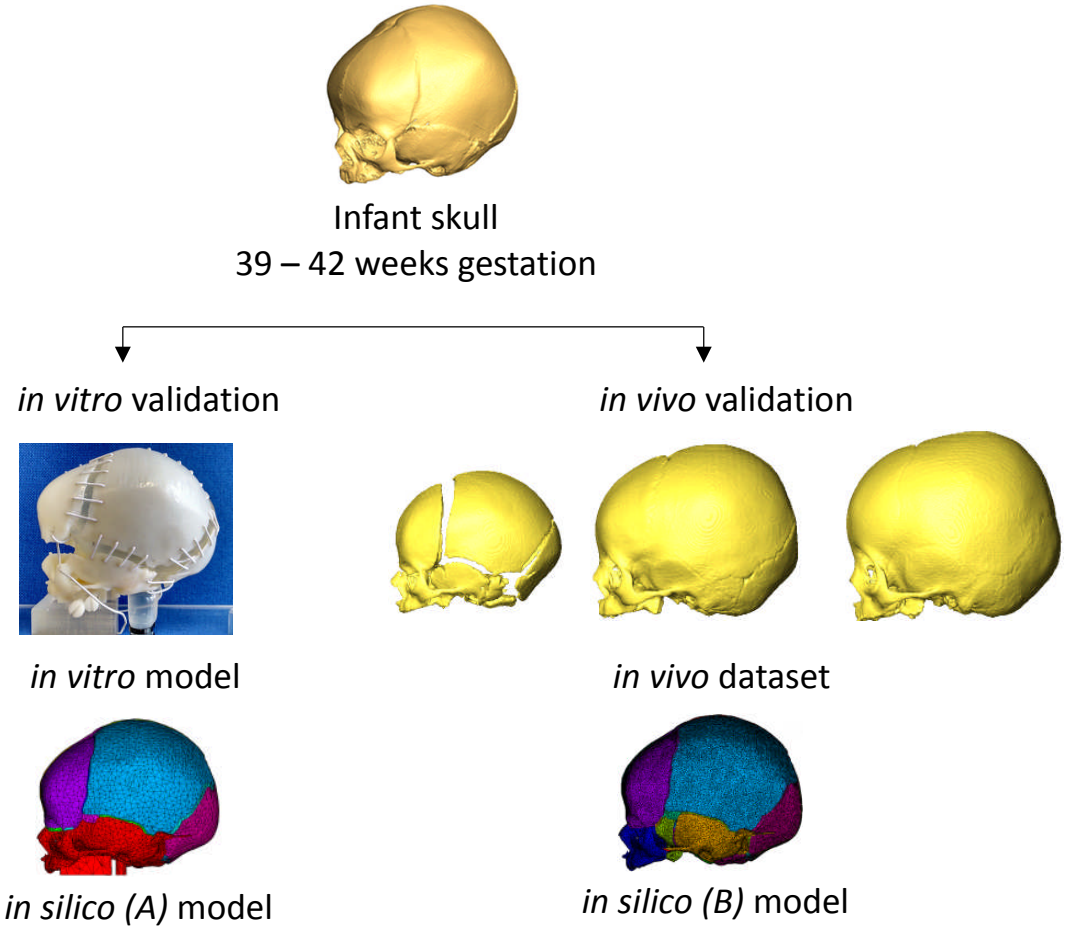

**Figure 2**. Orientation of the *in silico (B)* and *in vivo* skulls. The red line goes through the nasion and the subspinale and is the orientation of the skulls in this study. The Frankfort plane is shown in black and should be parallel to the ground for a normal head position. B) & C) show the *in silico (B)* seen in red and *in vivo* skull aligned with each other using the two orientations described.

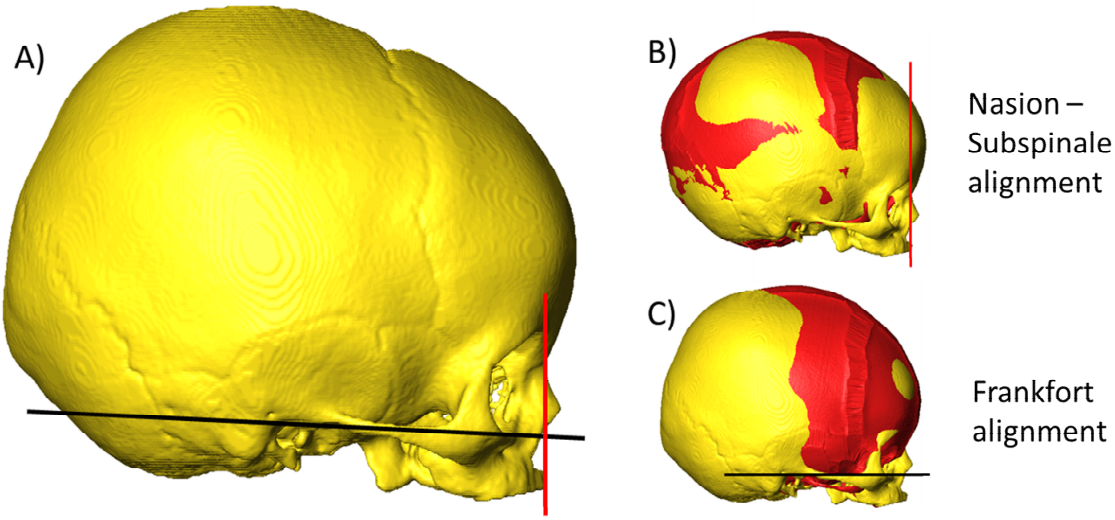

**Figure 3**: *in silico (A)* vs. *in vitro* physical model bar plots: The width, length and circumference parameters are recorded in the rows, while the female and male results are shown in the columns. Note the Y-axis does not start at 0mm.

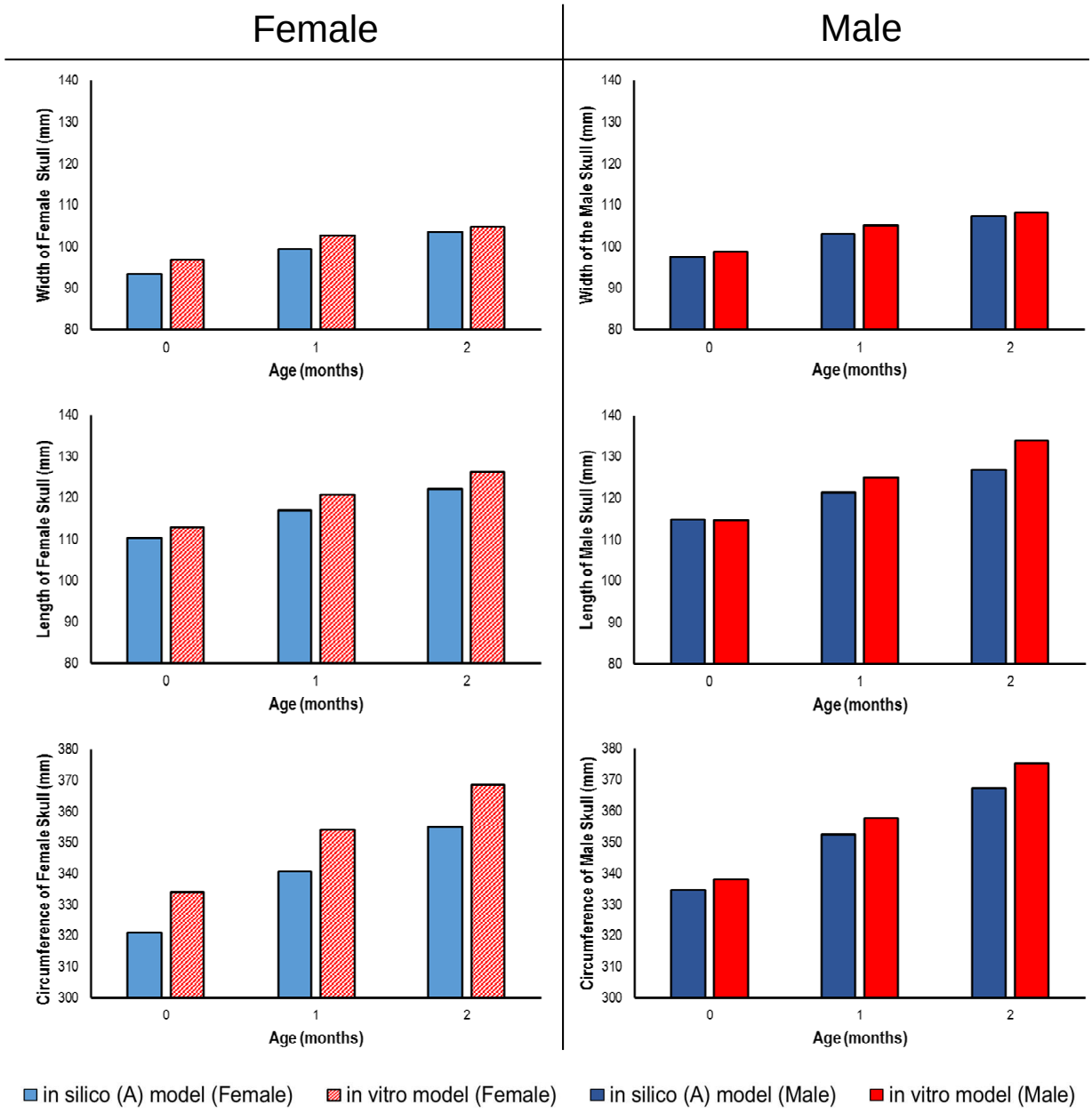

**Figure 4**. *in silico (A)* vs *in vitro* physical model: 3D distance plots. The red sections highlight where the *in silico (A)* model over-predicted the shape of the *in vitro* physical model, while the blue areas indicate where the *in silico (A)* under-predicted how the *in vitro* physical model expanded. Each skull has been scaled individually with the max and min scores for the colour chart given under each age.

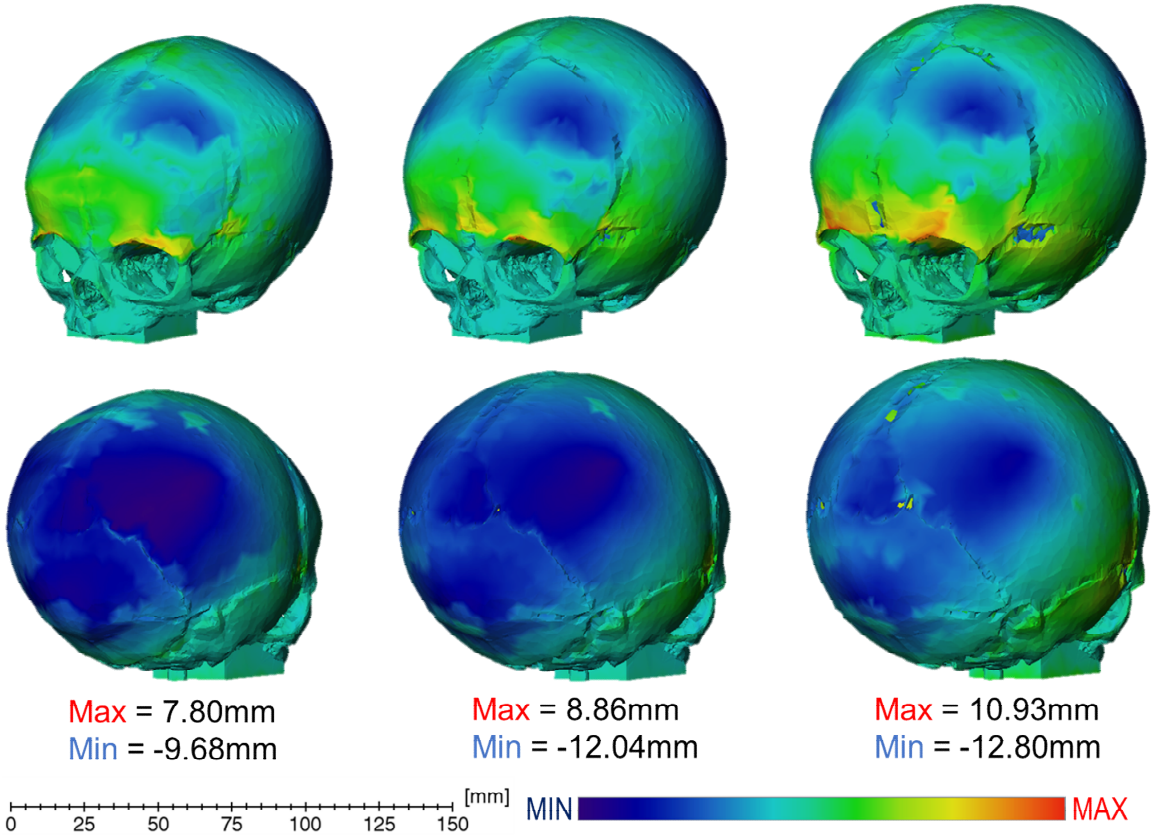

**Figure 5**. *in silico (B)* vs. *in vivo*: Width, length and circumference are shown in the rows while the columns show the female and male results for each parameter. The larger green rhomboid shapes are the *in vivo* 'average' skulls to which the *in silico (B)* model was compared against. Green = *in vivo* data, Light Blue = female *in silico (B)* models, Dark Blue = male *in silico (B)* models. Note Y-axis does not start at 0mm.

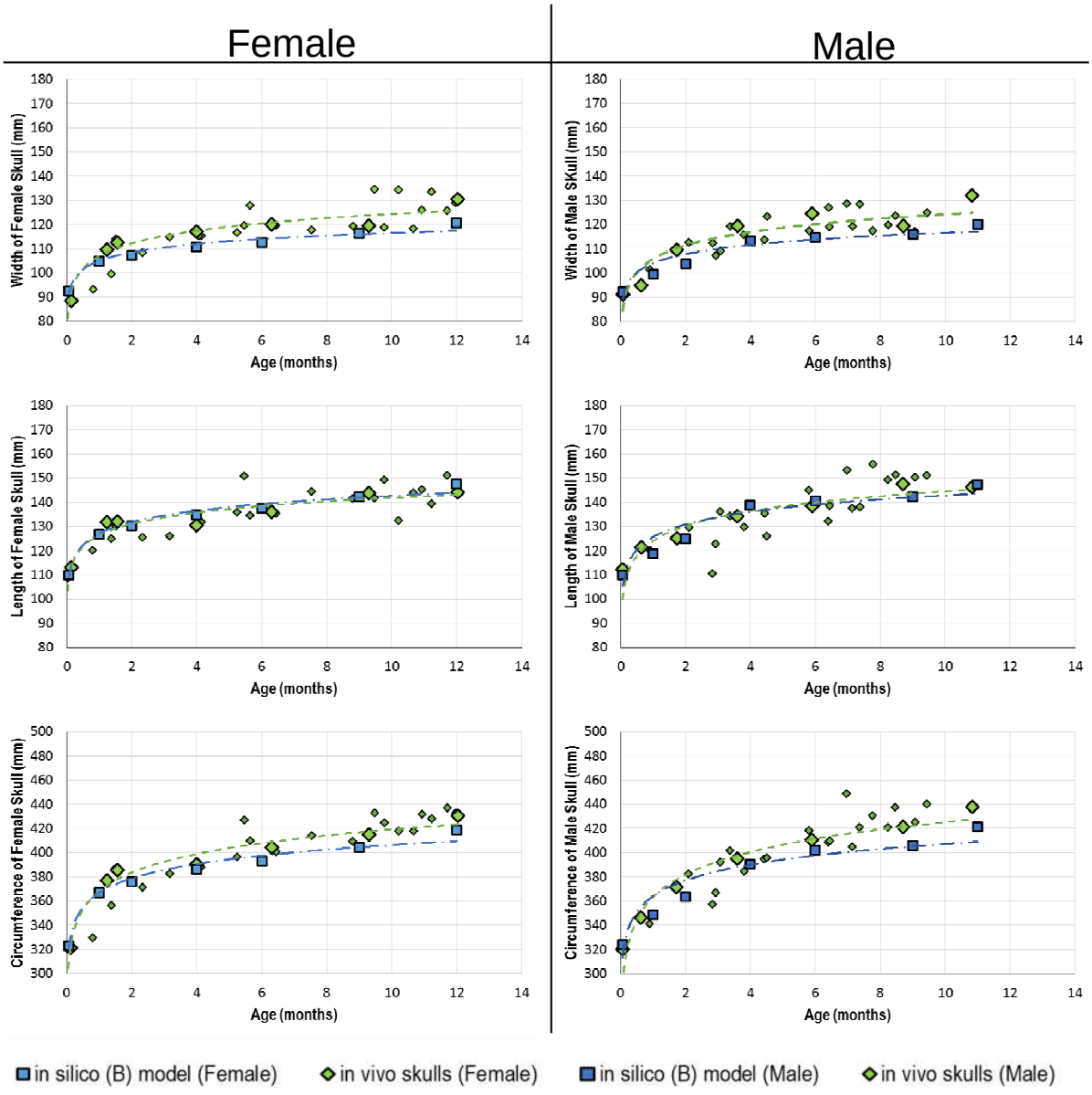

**Figure 6**. *in silico (B)* vs. *in vivo* - 3D distance plots: The blue areas on the plots highlight where the *in silico (B)* model under-predicted the *in vivo* CT data and the red areas indicate where the *in silico (B)* skull over-predicted the geometry of the *in vivo* CT data. Each skull has been scaled individually with the max and min values for the colour chart displayed below each age.

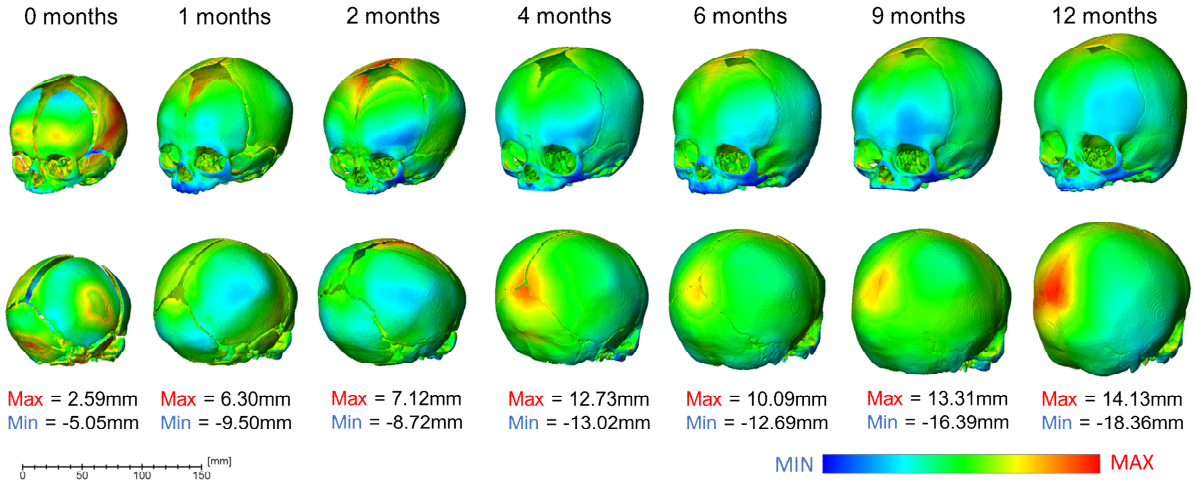

**Appendix 1**: Tables of *in vivo* skull measurements and ICV. Average skulls used are in bold.

| Skull number | Age category | Exact age in days | Gender | Width (mm) | Length (mm) | Circumference (mm) | ICV (ml) |
|---|---|---|---|---|---|---|---|
| **1** | **0 months** | **2** | **m** | **91.16** | **112.32** | **320.41** | **395** |
| **2** | **1 month** | **19** | **m** | **94.88** | **121.47** | **346.39** | **521** |
| 3 | | 27 | m | 101.31 | 120.25 | 341.16 | |
| **4** | **2 months** | **52** | **m** | **109.52** | **125.09** | **371.74** | **608** |
| 5 | | 63 | m | 112.74 | 129.7 | 382.69 | |
| 6 | **3 months** | 85 | m | 112.51 | 110.56 | 357.3 | |
| 7 | | 88 | m | 107.29 | 123.04 | 367.32 | |
| 8 | | 92 | m | 109.31 | 136.23 | 392.34 | |
| **9** | | **101** | **m** | **119.22** | **134.35** | **401.64** | **801** |
| **10** | **4 months** | **108** | **m** | **119.59** | **134.15** | **395.35** | **840** |
| 11 | | 114 | m | 115.82 | 129.74 | 384.87 | |
| 12 | | 133 | m | 113.65 | 135.56 | 394.93 | |
| **13** | **5 months** | **135** | **m** | **123.49** | **126.08** | **395.68** | **769** |
| 14 | **6 months** | 174 | m | 117.43 | 145.02 | 418.65 | |
| **15** | | **177** | **m** | **124.63** | **138.45** | **410.81** | **878** |
| 16 | | 192 | m | 126.99 | 132.29 | 408.68 | |
| 17 | | 193 | m | 119 | 138.64 | 409.89 | |
| 18 | **7 months** | 209 | m | 128.75 | 153.51 | 449.02 | |
| 19 | | 214 | m | 119.25 | 137.61 | 404.85 | |
| **20** | | **221** | **m** | **128.33** | **138.24** | **420.91** | **925** |
| 21 | **8 months** | 233 | m | 117.46 | 155.84 | 430.8 | |
| **22** | | **247** | **m** | **119.76** | **149.43** | **421.05** | **920** |
| 23 | | 254 | m | 123.58 | 151.44 | 437.38 | |
| **24** | **9 months** | **261** | **m** | **119.6** | **147.722** | **421.31** | **912** |
| 25 | | 272 | m | 117.16 | 150.55 | 425.11 | |
| 26 | | 283 | m | 124.98 | 151.18 | 440.32 | |
| - | 10 months | - | - | - | - | - | |
| **27** | **11 months** | **325** | **m** | **132.18** | **146.23** | **438.16** | **1017** |
| - | 12 months | - | - | - | - | - | |

| Skull number | Age category | Exact age in days | Gender | Width (mm) | Length (mm) | Circumference (mm) | ICV (ml) |
|---|---|---|---|---|---|---|---|
| 28 | **0 months** | 1 | f | 92.94 | 108.87 | 320.34 | |
| **29** | | **4** | **f** | **88.52** | **113.22** | **321.53** | **399** |
| 30 | **1 month** | 24 | f | 93.15 | 120.14 | 329.78 | |
| **31** | | **37** | **f** | **109.54** | **131.96** | **377.07** | **635** |
| 32 | | 41 | f | 99.75 | 125.18 | 356.66 | |
| 33 | **2 months** | 45 | f | 114.00 | 130.01 | 387.21 | |
| **34** | | **47** | **f** | **112.52** | **132.19** | **385.86** | **692** |
| 35 | | 70 | f | 108.54 | 125.60 | 371.53 | |
| **36** | **3 months** | **95** | **f** | **114.88** | **126.23** | **382.82** | **702** |
| **37** | **4 months** | **120** | **f** | **117.08** | **130.47** | **390.62** | **772** |
| 38 | | 124 | f | 115.52 | 132.05 | 387.89 | |
| 39 | | 122 | f | 115.41 | 130.67 | 391.07 | |
| **40** | **5 months** | **157** | **f** | **116.71** | **136.03** | **396.60** | **790** |
| 41 | | 164 | f | 119.72 | 150.87 | 427.23 | |
| 42 | **6 months** | 169 | f | 127.95 | 134.54 | 409.76 | |
| **43** | | **189** | **f** | **120.05** | **136.25** | **404.59** | **818** |
| 44 | | 193 | f | 119.56 | 135.57 | 401.13 | |
| **45** | **7 months** | **226** | **f** | **117.69** | **144.44** | **414.05** | **899** |
| - | 8 months | - | - | - | - | - | - |
| 46 | **9 months** | 264 | f | 119.53 | 141.63 | 409.29 | |
| **47** | | **279** | **f** | **119.44** | **143.92** | **415.07** | **915** |
| 48 | | 284 | f | 134.53 | 141.78 | 432.92 | |
| **49** | **10 months** | **293** | **f** | **118.94** | **149.42** | **424.71** | **956** |
| 50 | | 306 | f | 134.48 | 132.45 | 417.90 | |
| **51** | **11 months** | **320** | **f** | **118.39** | **143.90** | **417.86** | **945** |
| 52 | | 328 | f | 126.22 | 145.37 | 432.02 | |
| 53 | | 337 | f | 133.48 | 139.40 | 428.33 | |
| 54 | **12 months** | 351 | f | 125.76 | 151.13 | 437.15 | |
| 55 | | 359 | f | 129.10 | 147.86 | 432.85 | |
| **56** | | **361** | **f** | **130.61** | **144.21** | **430.54** | **1031** |

**Appendix 2.** *in silico (B)* vs. *in vivo* 3D distance plots – Frankfort plane alignment: The scaling polarity used here was the same as that used in Figure 6. The blue areas on the plots highlight where the *in silico (B)* model under-predicted the *in vivo* CT data and the red areas indicate where the *in silico (B)* skull over-predicted the geometry of the *in vivo* CT data. Each skull has been scaled individually with the max and min values for the colour chart displayed below each age.